Measurements of total and separated response functions of the deuteron through the quasielastic peak region for $q \approx 300-500$ MeV/c

B. P. Quinn,* A. M. Bernstein, K. I. Blomqvist,† S. A. Dytman,‡ and T. J. Pavel
Physics Department and Laboratory for Nuclear Science, Massachusetts Institute of Technology, Cambridge, Massachusetts 02139

R. M. Altemus,§ J. S. McCarthy, G. Mechtel,** R. R. Whitney,†† and T. S. Ueng
Physics Department, University of Virginia, Charlottesville, Virginia 22901

H. Arenhövel and W. Leidemann
Institut fur Kernphysik, Johannes Gutenberg-Universitat, D-6500 Mainz, Federal Republic of Germany

J. M. Laget
Service de Physique Nucleaire–Haute Energie, CEN Saclay, 91191 Gif-sur-Yvette Cedex, France
(Received 21 September 1987)

The cross sections for inelastic electron scattering from ^{2}H have been measured over a wide kinematic range covering momentum transfers q from approximately 250 to 600 MeV/c. To make longitudinal transverse separations of the response functions, both forward angle (60°) and backward angle (134.5°) data were obtained. The observations are in excellent agreement with calculations of Arenhövel and Leidemann and in slightly less good agreement with the calculations of Laget throughout the quasielastic peak and the "dip" regions.

INTRODUCTION

A striking feature observed in inelastic electron scattering spectra from the deuteron and all heavier nuclei is the broad "quasielastic" peak seen at approximately the final energy corresponding to elastic scattering from a free nucleon. This peak results from the scattering of the electron from a single nucleon moving within the target nucleus. In heavy nuclei, quasielastic peak cross sections have been well fit by a simple calculation in which the nucleon momentum distribution is taken from the Fermi gas model of the nucleus.[1] More recent experiments on heavy nuclei have obtained the Rosenbluth separation of the longitudinal and transverse response functions.[2,3] It appears that, although simple models can provide a good fit to the transverse contributions to the cross section over the quasielastic peak, they do not give good agreement with the observed longitudinal response functions. Furthermore, the dip in the transverse response function, between the quasielastic peak and the peak resulting from $\Delta(1232)$ production, is found to have consistently higher cross section than theoretical prediction, even when π-meson production and meson exchange current corrections are included. In the case of recent measurements[3] on ^{12}C, more sophisticated shell-model calculations have been found to give better predictions for the longitudinal response function, but at the price of poorer agreement with the transverse component. Although these calculations predict some filling in of the dip region, significant differences from the observed cross section continue to exist.

The data presented here on single-arm inelastic electron scattering from the deuteron represent part of a series of measurements of continuum inelastic electron scattering performed on light nuclei at the Bates Linear Accelerator Laboratory.[4,5] One objective of these experiments is to provide measurements which may show the onset of the observed effects which are presently unexplained in heavier nuclei, possibly shedding some light on the mechanisms involved. For example, within the framework of the shell model, if one considers pairs of nucleons which are not Pauli-blocked and so may have large spatial overlap, the number of such pairs of nucleons rises much more rapidly than A in these light nuclei. So discrepancies between measurement and simple calculations might also rise rapidly if the filling in of the dip is related to pairs of nucleons interacting strongly at short ranges. In general, these measurements on the simplest nuclei allow tests of the existing models in progressively more complicated systems.

The deuteron is obviously the simplest test case for which to check a model based on the picture of quasielastic scattering from nucleons within nuclei. Not only does it contain only two nucleons, but also they are weakly bound to each other so they may be expected to act more like free nucleons than those in any other nucleus. Furthermore, good nucleon-nucleon potentials are available[6,7] for generating realistic nuclear wave functions to be used in performing accurate calculations. The simplicity of the deuteron system is an even greater assest in performing more sophisticated calculations which include final state interactions, meson-exchange currents, and meson production. The deuteron might not provide a strong test of current theories of nucleon modifications within the nucleus, since the weak binding and associated diffuse wave function may make these corrections rela-

tively small. On the other hand, a failure of such a complete calculation to predict the observed longitudinal and transverse response functions would suggest an underlying error in the basic assumptions. A change in the behavior or form-factor of the nucleons when bound or even a breakdown of the model of nuclei as collections of nucleons might, for example, then be indicated. This would then have to be resolved before there would be any chance of understanding the existing difficulties in heavier nuclei. So a logical first step toward undestanding the observed differences between calculations and actual behavior in heavy nuclei is the measurement of the response functions of the deuteron over the same kinematic region in which problems exist in explaining results found for heavier nuclei. Progressively more challenging tests of the calculations can then be made by measurements on $A=3$ and 4 nuclei.

The earliest measurements of electron scattering from the deuteron in the quasielastic region were made specifically for the purpose of determining the electromagnetic form-factors of the neutron.[8] Therefore, sensitivities to the deuteron wave function or to final state interactions (FSI) between the outgoing nucleons were viewed as background effects which were to be minimized if possible. With this view in mind, the early dispersion theoretical calculations of Durand[9] were expanded upon by several authors[10] who included the effects of FSI for the purpose of correcting the data for this effect. In particular, Durand's calculation was refined by McGee[11] to include D state contributions and additional relativistic effects and expanded to included FSI.[12] The results of these calculations were used in the analysis of the abovementioned experiments in attempting to correct for FSI effects and to aid the development of the best method of extracting $G_n^M(q)$ and $G_n^E(q)$. Measurements, therefore, generally concentrated upon determining the height of the quasielastic peak and its ratio to the ^{1}H elastic cross section or ratios of cross sections tagged by coincident neutrons or protons, rather than determining the detailed shape and magnitude of the response surface.

Other effects which were considered difficult to calculate at the time of these early measurements were contributions to the response functions due to nucleon resonance effects and meson exchange currents (MEC) in excess of those included via the Siegert terms in the original Durand[9] calculations. It was largely to avoid MEC contributions that the peak height of the quasielastic spectrum was often chosen as the quantity to be measured for extraction of G_n. When calculations of these effects became available,[13] new high-accuracy measurements were undertaken across the quasielastic peak[14] at selected kinematics, and particularly in the threshold region[15] to determine whether the actual MEC effects matched the predictions. With this first opportunity to actually perform a clear measurement of meson exchange within a nucleus, the interest was now upon the detailed comparison of theoretical calculations with the observed nuclear properties, rather than simply in using the spectra to extract the properties of the nucleon. Simon *et al.* compared their measurements at Mainz[14] to calculations by Fabian and Arenhövel and found the predictions to be accurate across the entire peak for the two cases studied, although examination of their results suggests a systematic tendency for the measurements to fall 3% to 4% below the prediction at beam energy of 300 MeV and scattering angle of 90°. Subsequent measurements[15] permitted the separation of the longitudinal and transverse form-factors in the threshold region and showed excellent agreement with the predictions of Fabian and Arenhövel, which included a large MEC contribution to the transverse response function in this kinematic region.

Laget[16–18] has applied to the calculation of electron scattering from the deuteron the same type of diagrammatic calculations as he has used for photo-pion production and photo-disintegration calculations. In view of the favorable situation of having several methods of predicting the cross section for this reaction, it is appropriate to make measurements over a wide kinematic range to test these theories as well as possible.

Previous measurements on the deuteron have not mapped out enough of the kinematic plane to allow the data to be unfolded to generate the cross sections in the absence of radiative effects without model dependence. Rather, to compare calculations with the observed spectra, it has been necessary to fold the radiative effects, and often instrumental resolution, into calculations or to use models of the cross section to make estimates of the radiative corrections required on the data. More significantly, the data presented here represent the first set of measurements to be taken on the deuteron at two different angles over this kinematic region to allow separation of the longitudinal and transverse contributions to the response function over the quasielastic peak and the dip region.

THEORY

In single-arm electron scattering, the measured quantities are the incident electron energy, E, the scattered electron energy, E_f, the scattering angle, θ, and the double-differential cross section in the presence of radiative effects, $(d^2\sigma/d\Omega\, dE_f)_{\rm rad}$. These determine the energy loss, $\omega=E-E_f$, the momentum transfer, $q=[E^2+E_f^2-2EE_f\cos(\theta)]^{1/2}$, and the four-momentum transfer,

$$q_\mu^2=\omega^2-q^2=-4EE_f\sin^2(\theta/2)\ .$$

Since the electromagnetic coupling constant is small, it is a good approximation that, for nuclei with $Z\ll 137$, the electron interacts with the struck nucleus through the exchange of a single virtual photon with energy, ω, and momentum, q. Thus even in the highly inelastic region, the interaction is weak in this sense. This is one of the major advantages of the use of electrons, rather than hadrons, to explore the behavior of nuclei. It can be shown[19] that within this approximation, and assuming parity conservation, Lorentz invariance, and gauge invariance, the cross section can be written in terms of two angle-independent functions, $R_L(q,\omega)$ and $R_T(q,\omega)$, as

$$d^2\sigma/d\Omega\, dE_f=\sigma_M\{(|q_\mu^2|/q^2)^2R_L + [\tfrac{1}{2}(|q_\mu^2|/q^2)+\tan^2(\theta/2)]R_T\}\ ,$$

where $\sigma_M = \alpha^2 \cos^2(\theta/2)/[4E^2 \sin^4(\theta/2)]$ is the Mott cross section.

The functions $R_L(q,\omega)$ and $R_T(q,\omega)$, the longitudinal and transverse response functions, then contain all the information that can be determined about the nucleus in a single-arm experiment. Since the exchanged photon has a nonvanishing four-momentum transfer, q_μ, the virtual photon can be longitudinally polarized in contrast to real photons which can only have transverse polarization. It is the exchange of longitudinally polarized photons which gives rise to the term containing R_L, corresponding to scattering events in which the component of angular momentum along q is not changed. The experimental values of R_L and R_T can be obtained from sets of data taken over the same section of the q-ω plane at different scattering angles by a Rosenbluth separation. That is, a straight line fit to

$$(q^2/|q_\mu^2|)^2(d^2\sigma/d\Omega\, dE_f)/\sigma_M$$

versus

$$(q^2/|q_\mu^2|)^2[\tfrac{1}{2}(|q_\mu^2|/q^2)+\tan^2(\theta/2)]$$

will yield a slope equal to $R_T(q,\omega)$ and an intercept of $R_L(q,\omega)$.

In the framework of the basic quasielastic model, where the nucleon absorbing the virtual photon is ejected while the residual nucleons are merely spectators, the cross section for scattering with the transfer of a given momentum and energy would just be a measure of the probability of finding a nucleon within the target nucleus with the right initial kinematics to absorb the transferred quantities and then be on the mass shell. The longitudinal and transverse response functions and the overall cross section would each just reflect this same probability distribution, modified by the form factors of the constituent nucleons, so the separation would provide no new information. The situation remains similar if, in the final state, the outgoing particles interact with each other. The response surfaces will be distorted, so they are no longer simply based upon the nucleon probability distribution, but the expected response functions could, in principle, still be calculated in terms of the nucleon form factors. The separation might then be useful in determining the electromagnetic form factors of the neutron which cannot be measured directly. This technique has been used[8] in the past but the necessary approximations are better in a higher momentum transfer region than that of the present experiment.

In reality, effects other than simple quasielastic scattering are known to contribute to inelastic scattering from the deuteron, lending greater significance to the separation of the response function. Previous experiments have shown[14,15] significant contributions to the electromagnetic structure of the deuteron from currents arising from the exchange of charged mesons between the two nucleons. These meson exchange current effects, which are found to be quite substantial in the threshold region at low momentum transfer, are expected to contribute almost exclusively to the transverse response function, providing a clear tag of a process which is not simply quasielastic in nature. Similarly excitation of the $\frac{3}{2}^+$ $\Delta(1232)$ is mainly through an unnatural parity, 1^+, transition. Since the longitudinal photons are of natural parity, the large Δ peak may be expected to show up in the transverse response surface much more than in the longitudinal. Separation of the response functions for the deuteron and other light nuclei may similarly be expected to give a clue to the nature of the effects responsible for such unexplained phenomena as the filling in of the dip region. As stated above, separation of data for heavy nuclei has indicated the existence of a problem in the understanding of the longitudinal response functions of heavy nuclei despite initial success in fitting cross sections at a single angle.

It is important to note that the observed cross section $(d^2\sigma/d\Omega\, dE_f)_{\rm rad}$ will differ from the true scattering cross section in that the electrons will emit real photons both before and after scattering, both in the field of the struck nucleus and in the fields of other target atoms. Determination of the true cross section, $d^2\sigma/d\Omega\, dE_f$, from the observed cross section requires complex radiative correction procedures, which will be described in the analysis section.

EXPERIMENTAL PROCEDURE

The experiment was conducted at the Bates Linear Accelerator Center using the energy-loss spectrometer system (ELSSY). A 20 μA beam of electrons of a selected energy was passed through a pressurized deuterium gas target cell, and electron-scattering rates were measured at a selected angle over a wide range of final energies. The 13 incident-energy and scattering-angle combinations measured are listed in Table I. As the momentum acceptance of ELSSY is only $\approx 6\%$ of the central momentum, a series of central momenta were measured to map out the cross section as a function of energy loss. Figure 1 shows the region of the (q,ω) plane covered at each scattering angle. Scattering rates for ^{1}H, ^{3}He, and ^{4}He and an empty target cell were also measured over the appropriate final-energy ranges by sequential measurements at each central momentum setting.

TABLE I. Kinematics of the experiment. E (central) denotes the electron energy at the center of the target in MeV with a $\pm 0.15\%$ error.

θ	E (central)
60°	292.8
60°	365.6
60°	465.3
60°	510.2
60°	596.8
90°	223.8
90°	287.8
134.5°	174.3
134.5°	233.1
134.5°	278.5
134.5°	327.7
134.5°	367.7
134.5°	444.2

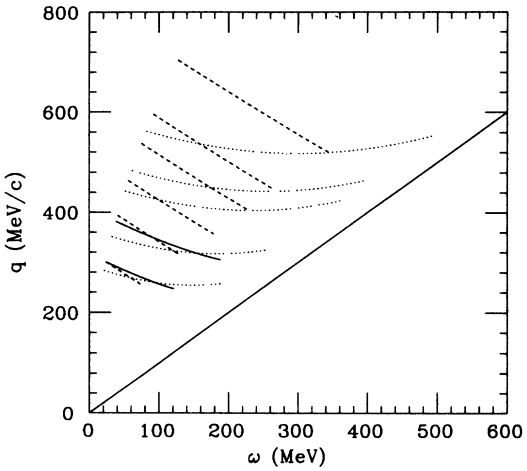

FIG. 1. The kinematic region covered in this experiment is shown in the (q,ω) plane. The horizontal axis is the energy lost by the electron, the vertical axis is the three-momentum transferred. Note that kinematics require $q > \omega$ so the region below the 45° line is unphysical. Each curve shown represents a single combination of incident energy and scattering angle. The positions along the curve were scanned by changing the spectrometer momentum setting. The dotted lines represent 60° measurements, dashed lines are at 134.5°, and solid lines are at 90°. Rosenbluth separations can be performed in the regions in which measurements at different angles overlap.

The targets, shown in Fig. 2, were cylinders 1 in. in diameter and 9 in. in length, oriented so the beam passed along the axis. The entrance and exit windows were composed of copper-coated steel, each with a total thickness of 1.5% of a radiation length. the scattered particles passed through side walls of 20 mil stainless steel which presented ≈3% of a radiation length at normal incidence. The targets were sealed units, permanently pressurized to 100 atom at 20 °C. To prevent over pressurization due to beam heating, the targets were cooled with liquid nitrogen while in the beam. Two sets of horizontal slits between the target and spectrometer ensured that only particles originating from the central region of the target had an unobstructed path into the spectrometer. To first order this excluded from the spectrometer all electrons which scattered in the windows and eliminated all scattered electrons which would have hit the magnet pole faces.

Scattered electrons, columnated by the horizontal slits and one set of vertical slits, entered the spectrometer without encountering any intervening material other than the target. Those with the selected momentum were then bent down 90° to the focal plane detectors, arranged as shown in Fig. 3, in a heavily shielded pit. The detectors were a vertical drift chamber (VDC) which measured position and angle along the dispersion direction; a pair of proportional chambers, the transverse array (TA), which measured position transverse to the dispersion direction; an Aerogel ($n = 1.05$) Cerenkov detector (C3) which was used to eliminate contamination from other particles, such as pions and their decay muons; and two lucite Cerenkov detectors (C1 and C2) which provided some redundancy and an auxiliary trigger. The trigger for scattered electrons was a coincidence between C3 and either C1 or TA. Events with only C1-TA coincidences were also recorded to monitor background from pions and muons and to check the efficiency of C3. The information which was read from these detectors and stored event by event included the pulse size and time for all three Cerenkovs, a pair of delay-line times for the TA to indicate position and drift time, and three pairs of delay-line times for the VDC to indicate position and drift times for the three wires closest to the track.

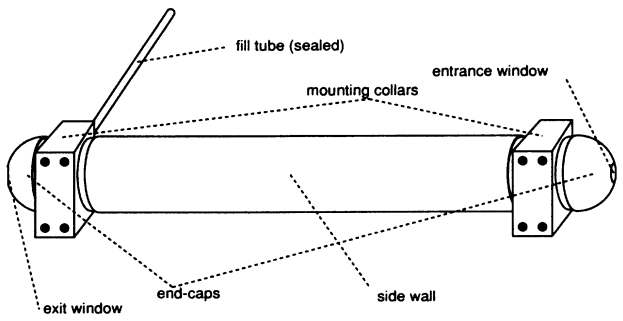

FIG. 2. A target vessel is shown. Identical vessels were used for each gas and an additional empty target was used for background measurements. Each target was pressurized then permanently sealed. The beam passed along the axis of the cylinder, entering and exiting through thin windows.

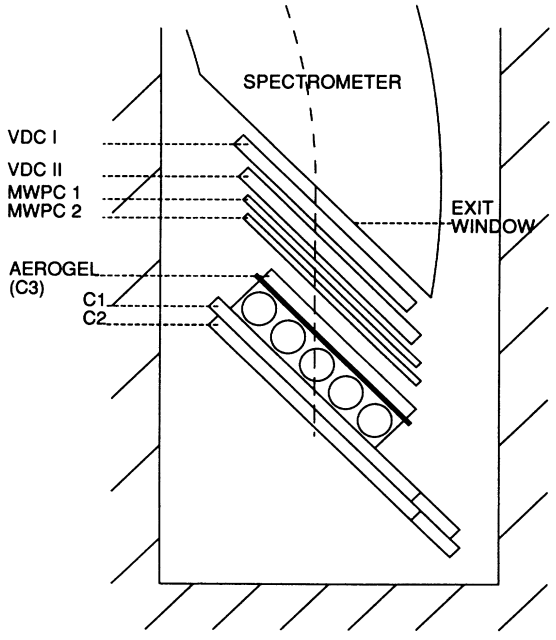

FIG. 3. The arrangement of the detectors at the spectrometer's focal plane is shown. Scattered electrons, bent down by 90° into the shielding pit, enter the detectors from above, as shown. See the text for descriptions of the detectors and their uses.

The first order optics of the ELSSY spectrometer are parallel to point in the transverse direction and point to point in the dispersion direction. Thus positions in the TA and VDC measure initial horizontal angle and scattered momentum, respectively. The horizontal angle spectrum proved to be useful for background suppression since the expected distribution of horizontal angles could be calculated from geometrical considerations and compared to the observed distribution. In preliminary runs it was observed that horizontal angle spectra found at low final momentum differed significantly from the expected shape. Investigation disclosed a background source from multiple scattering in the vacuum vessel. This problem was eliminated during actual data acquisition by the use of redesigned vacuum containment.

Preliminary runs also indicated that the effective target thickness decreased, because of expansion of the struck gas column, if the beam peak current density was very high. During data collection the beam was slightly defocused and its peak current was limited to ≈ 4.5 mA to prevent these thermal effects. The success of this precaution was monitored by recording the time within the beam burst of each event and the instantaneous beam current at the time of the event. The scattering rate was found to be directly proportional to the instantaneous current and independent of the time within the burst.

ANALYSIS

Elastic scattering cross sections were measured for ^{1}H at all energy-angle settings and for ^{2}H, ^{3}He, and ^{4}He at eight settings where the required counting times were not prohibitive. These cross sections, which were determined from the data in essentially the same manner as the inelastic cross sections, were compared to previous measurements to check the normalization of the data. An overall normalization factor of 1.06 ± 0.03 was determined principally from the comparison of the ^{3}He elastic scattering cross sections to a recent measurement.[20] Comparison of elastic scattering cross sections on ^{1}H to a fit to the world's supply of data[21] also gave a very similar normalization factor. Estimation of the systematic errors in this factor are discussed in the next section. The elastic data, especially on ^{1}H, also provided a test of radiative correction parameters and procedures. In calculating the true cross section of a peak, the observed differential cross section across the peak is integrated to some cutoff energy below the peak's central energy. A correction factor for the remaining radiative tail at still lower energies is then calculated and applied. For cutoff energies more than a few MeV below the central energy, the value of the radiatively corrected elastic cross section was found to be independent of the cutoff energy used in calculating it, as it should be if the calculated corrections properly match the actual radiative effects. Finally, the position of the elastic peaks in the final-energy spectrum gave a calibration of the spectrometer constants and the beam energy at the center of the target.

Since single-arm inelastic scattering measurements are potentially very susceptible to background effects, the event-by-event data were subjected to a series of cuts and corrections intended to eliminate background contributions as much as possible. Before these cuts, background contributions were a few percent in the quasielastic peak region and somewhat larger for points at very low final energy in the dip region. The normalization factor of 1.06 determined from the elastic peaks should correct for real events inadvertently discarded by these cuts.

One source of background, which was significant at low momentum, apparently resulted from large numbers of low energy particles produced by annihilation of negative pions in the spectrometer's baffles. This flat background was eliminated by requiring that all events give a large pulse in at least one of the trigger Cerenkovs, C1 and C3. The resulting loss of efficiency was about 1%.

Pions and muons were rejected by a cut on the Aerogel Cerenkov pulse size. Except at the highest spectrometer settings, pions and muons of the selected momenta had velocities less than the critical β value of $\beta_{\text{crit}} = 1/1.05$. Even for the few spectrometer settings which did have $\beta_{\text{pion}} > \beta_{\text{crit}}$, the rejection efficiency was high while the background flux was small. No measurable fraction of the accepted events failed to fire C1 at momenta below C1's pion threshold, indicating that the rejection efficiency of C3 was well over 99%.

No correction was made for electrons resulting from electron-positron pair production since calculations showed such production to be negligible in the kinematic region of interest for nuclei with atomic number $Z = 1$ or 2. Some positive polarity measurements were made to test background suppression. The contribution was found to be completely negligible except at the lowest momenta, where it could be as much as 5% of the normal polarity signal, possibly resulting from secondary particle production by the main scattered beam which was then being dumped at the top of the spectrometer.

The largest background contribution which had to be removed was that arising from the target vessel itself. This was measured directly by placing an empty sealed vessel in the beam. In regions where the contribution from this blank target was large, this measurement was performed both before and after the gas target measurements. The count rate from the empty target was generally negligible for measurements across the quasielastic peak but grew very rapidly at decreasing final momentum, sometimes exceeding the signal for final momenta less than ≈ 90 MeV/c. The focal plane transverse position (TA) spectra for low momentum blank target runs showed a flat component, coming from uncollimated sources, and a small peaked component produced by large-angle scattering from the target's side walls of beams particles initially deflected by the entrance window. Therefore, not only was the blank target contribution subtracted from the count rate for calculation of cross sections, but also its contribution to the TA spectrum was subtracted channel by channel from that of the gas target measurements to determine a corrected TA spectrum, as illustrated in Fig. 4.

Similar background contributions would also be generated by the gas itself in the gas targets. The precise size of this contamination is difficult to ascertain although upper limits can be placed upon it. The contribution

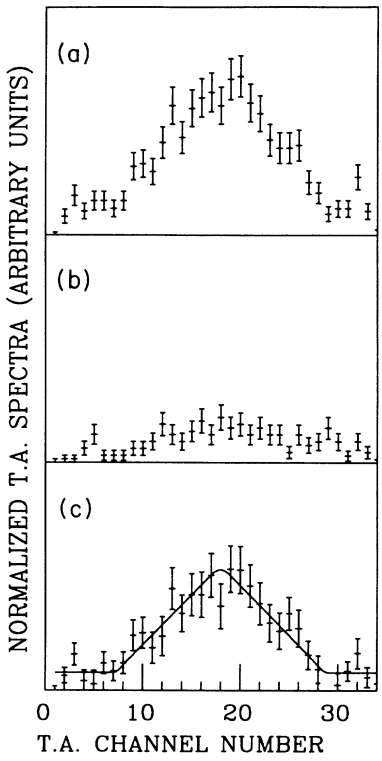

FIG. 4. (a) A transverse array (TA) spectrum for particles detected while a deuterium target is in the beam. The TA measures position in the direction transverse to the bend plane. With the parallel-to-point optics of the spectrometer and the known slit collimation, the expected distribution of particles scattered from the gas can be calculated to be a slightly skewed trapezoid. The plot shows a particularly low momentum spectrometer setting, so background contamination is relatively severe. The background contribution falls rapidly with increasing scattered momentum and is negligible across the quasielastic peak. (b) Same as (a) but for an empty target in the beam. All counts here are contributed by background effects. The peaked component is believed to originate from scattering of electrons in the walls of the target. The peaking is introduced by the collimation by the slits. (c) The difference of (a) and (b). The remaining flat background is induced by the gas. The solid line is a two parameter fit to the spectrum as the sum of the predicted trapezoidal shape and a flat background.

from the gas should, for example, be significantly less than that from the empty vessel, first because the thickness of gas encountered by the beam is less than the thickness of the metal windows, and second because the angle of scattering required to deflect beam particles into the side wall is generally much larger from a point within the gas than from the entrance window. Since this undetected background is expected to be a small fraction of the detected background, a strong upper limit can be set on this contamination by discarding all data points for which the blank target rate exceeded 20% of that from the gas target. In practice, this set the lower limit for scattered momentum since the blank contribution rose monotonically and rapidly with decreasing final energy as in the example shown in Fig. 5.

Furthermore, it was possible to eliminate a large part of this gas-induced background contribution from the observed count rate. The background arising from neutral particle production in the gas, as well as from other uncollimated sources such at π^- annihilation in the spectrometer, is expected to have a flat TA spectrum. On the other hand, the signal, collimated by the horizontal slits, is expected to have a known characteristic shape. A final level of background suppression was therefore achieved by performing a two-parameter fit to the blank-subtracted TA spectra as the sum of a flat background component and the component of known shape. The flat component was then subtracted from the count rate. One such fit is shown in Fig. 4(c) for a low-momentum point with particularly high contamination. Good values of χ^2 were obtained indicating that the background component was indeed flat. The resulting correction never exceeded 20%, and decreased rapidly with increasing final momentum. The correction was negligible over the quasielastic peak.

A simple dead time correction of 1–2 % was calculated from the ratio of actual triggers to events recorded. An additional measured correction factor was included to compensate for tracks which were corrupted. Because of the large flux of very low energy charged secondary particles present at low field settings, this latter correction was sometimes as large as 7% or 8%.

The central region of the spectrometer's momentum bite, where the detectors has a uniform efficiency, was divided into one, two, or three bins, with a total momentum bite of about 4.5%. The contribution from the blank target was subtracted bin by bin after scaling the counts by the number of incident electrons. The counts in each bin were then corrected for the fraction of flat background in the corresponding blank-subtracted TA spec-

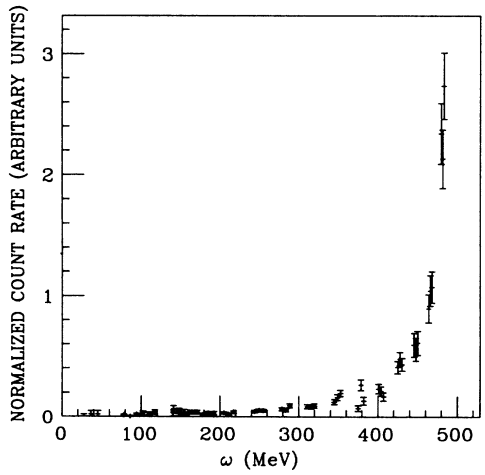

FIG. 5. A typical spectrum from a blank target is shown, in this case 598 MeV beam energy, 60° scattering angle. Count rates were normalized to the amount of incident beam, then subtracted from the gas target count rates. The count rate is seen to rise steeply at scattered electron energies near or below 100 MeV.

tra. These corrected counts were then converted into a double differential cross section using the known momentum bite for each wire, gas density, vertical angular acceptance, calculated acceptance integral of the horizontal slits, and incident number of electrons.

The contribution of the radiative tail of the elastic peak was calculated[21] using a parametrization of the measured elastic cross section,[22] then subtracted from the double differential cross section. This correction was never more than a few percent for final energies below the breakup threshold. Good agreement was found between the predicted elastic tail on ^{1}H, found by calculating radiative effects on previous elastic cross section measurements,[23] and the values measured in this experiment below pion-production threshold, see Fig. 6. This agreement confirms the accuracy of the model of the target used in the calculations and of the calculation method, as well as demonstrating that this region of the spectrum was free of unexpected contamination. This check was the main reason for performing simultaneous measurements on ^{1}H.

Unfolding of the measured cross sections was necessary to determine the actual cross sections in the absence of radiative effects. These changes in the observed spectrum can be divided into two effects. First, the number of electrons observed in an arbitrary energy and angle bin will be reduced by a radiative correction factor because photon emission will deflect some electrons or change their energy, before or after scattering, enough to remove them from the bin of interest. Secondly, a continuum radiative tail cross section will be added because photon emission will deflect some electrons into the bin of interest, either by changing the total deflection angle or by increasing the apparent energy loss.

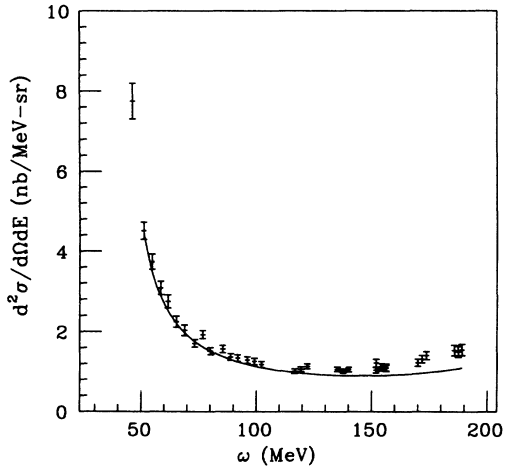

FIG. 6. A series of measurements of the ^{1}H cross section is shown. In the region below the pion-production threshold only the radiative tail of the elastic peak contributes. The solid line shows the predicted radiative tail found from the formalism of Mo and Tsai (Ref. 21) and a parametrization of previous ^{1}H elastic scattering cross sections (Ref. 23). The agreement is found to be good, indicating that the radiative properties of the target are well understood and that no unexpected background exists.

In principle, the latter term will depend upon the true cross section at energies and angles other than those of interest. Fortunately, it has been shown[21] that an angle-peaking approximation may be used since bremsstrahlung is strongly forward peaked. In this approximation, the tail term results only from electrons which scatter at or below the beam energy through the angle of interest to final energies at or above the observed final energy. While this simplification is sufficient for calculation of tail contributions from discrete transitions, such as elastic scattering, an additional approximation is made in the calculation of the continuum radiative tail. This energy-peaking approximation[21] is based upon the fact that most of the energy lost to radiation will, in fact, be carried by a single photon. Then the significant contributions to the continuum radiative tail come either from electrons which scatter at the beam energy and then drop to the observed energy by emission of a photon, or from electrons which lose energy by photon emission and then scatter to the final energy and angle. Since cross sections tend to increase rapidly with decreasing incident energy, the latter contribution can be quite large.

Thus given the true cross section at some angle the observed cross section at that angle can be predicted using the calculations of Mo and Tsai and parametrizations of the bremsstrahlung probability within the target, by multiplying the true cross section at any final energy by a calculated radiative correction factor, and then adding the calculated tail cross section for that final energy. Reversing the process, to unfold the true cross section from an observed cross section, is a more complicated iterative procedure, which will be discussed below, but is based upon the same approximations and calculations. These corrections required a method of parametrization of the cross section over the entire q-ω region of interest to allow the cross sections to be used to generate a series of progressively more accurate approximations of the corrections.

The parametrization at a given angle was generated from the data points at that angle by the following method. Smooth curves, a Gaussian plus polynomials, were fit to each set of points at a given beam energy. These provided a continuous distribution of cross sections at all values of ω. To eliminate the beam energy dependence of the inelastic spectra, cross section curves were than scaled by dividing out the sum of the elementary nucleon cross sections at that q and θ and by dividing out a kinematic factor, dY/dE_f where Y is the "scaling variable," $Y=m_N\omega/q-q/2$. To extend the parameterizations to the rest of the q-ω plane, interpolation and extrapolation were done along lines of constant Y for ω below the pion-production threshold and along lines of constant invariant mass of the nucleon plus virtual photon, $m^2=(m_p+\omega)^2+q^2$, for higher ω. This selected paths of constant feature over the quasielastic and Δ production peaks. For q-ω points which lay between two incident energy curves, a straight-line interpolation was done between the two parametrizations. For points at lower q than any measured value, extrapolation was performed with a straight-line fit to all available parametriz-

zations along the extrapolation path. In either case, the derived value was then converted back to a cross section by multiplying by the scaling factors applicable for that q, ω, and θ.

This prescription provided cross section estimates for all q-ω points located at a lower q than the highest-energy measurements at the particular angle and ω. This was sufficient to perform radiative unfolding within the angle-peaking approximation.[21] The cross section actually required in calculating these corrections is the true cross section in the absence of radiative effects. Since those were not available in advance, an iterative technique was used. The measured cross section was used as a first approximation to the true cross section. Using the fitting and interpolation methods described above and the results of Mo and Tsai, it was possible to estimate the continuum radiative tail contributions that would be expected at each of the measured points. This was subtracted at each point and the resulting value was divided by the calculated radiative correction factor to yield a second approximation to the unfolded cross section. This was in turn fit and extended over the q-ω plane to allow still better calculation of the radiative tail contributions. These were again subtracted from the original measured values and the radiative correction factors were applied. This process could have been continued until it converged but convergence was accelerated by averaging these second and third approximations. Two more iterations were then performed and their results were also averaged. At this point the procedure was found to have converged. A final iteration was performed with the statistical errors on the data points being propagated through the subtraction and multiplication. This gave an estimate of the statistical errors on the corrected cross sections.

As an internal consistency test of the measurements, data analysis, and error assignments, interpolations of the unfolded cross sections to the $q=300$ MeV/c line were performed for all three angles measured 60°, 90°, and 134.5°. Rosenbluth separations were then performed at a set of ω values ranging from 30 to 140 MeV. At each of these points the three values used in the separation were found to lie very well on a straight line, except at $\omega=40$ MeV where a 3.6 σ deviation was found, possibly resulting from a nonstatistical error introduced in the interpolation. Data at 90° were only available over a small part of the kinematic region covered so it was used only as a check, and not included in the final separations. To avoid introducing unacceptable systematic errors in the final results, the data taken at 134.5°, which had poor statistics, were not interpolated to other q-ω points before separation. Rather, the 60° data were interpolated to the q-ω points at which back-angle measurements were available and Rosenbluth separations were performed. Very near the breakup threshold, interpolation was complicated by the fact that variation of the cross section was not smooth along lines of constant scaling variable, Y. To avoid potentially introducing large systematic errors, separations were not performed at points which would require interpolation across the breakup threshold. The resulting separated longitudinal and transverse response functions at the kinematic points of the 134.5° data will be presented in the next section.

DISCUSSION

Numerical calculations for quasielastic scattering from the deuteron in the kinematic region of the experiment were performed by us using the prescription provided by McGee[11] and bound state solutions to boundary-condition model potentials of Lomon and Feshback.[6] Final state interactions were not included in this calculation, as the calculation was intended only as a relatively simple test to determine the sensitivity of the cross section to various parameters. The formalism for these corrections was presented by the same author[12] but is quite complex. The formalism used by McGee was a dispersion theory approach and provided a covariant description of the reaction but used a nonrelativistic deuteron wave function.

Some of the results of our calculations are shown in Fig. 7, which shows part of a study of the sensitivity of the cross section to the neutron magnetic form-factor. The effect of a significant change in G_n^M is seen to be small, even at back angles. Comparison with the data, presented below, will show that an improvement upon present measurements of G_n^M is outside the scope of the present measurement simply because of the statistical uncertainties of the measured points. Conversely, this weak dependence indicates that no significant discrepancies between experiment and calculation can be expected to result from the small uncertainties in the magnitude of G_n^M

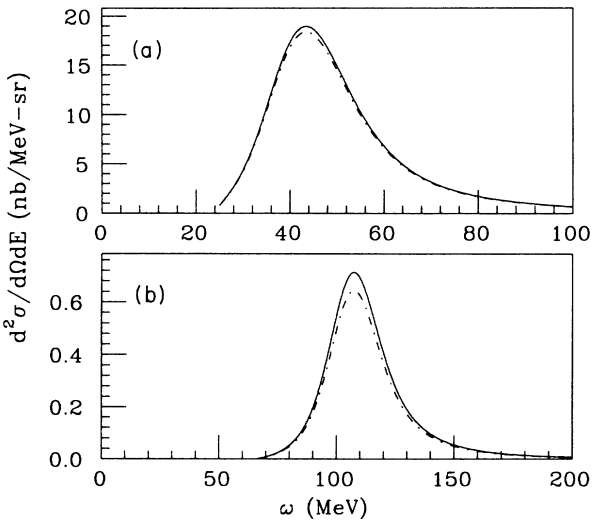

FIG. 7. (a) The solid curve shows the prediction of McGee (Ref. 11) for the quasielastic scattering cross section from the deuteron at 300 MeV and 60°. The magnetic form-factor of the neutron, $G_n^M(q)$, assumed in the calculation, is from a fit to previous measured cross sections (Ref. 23). The dot-dashed curve shows the same thing except that $G_n^M(q)$ has been reduced by 20% for all q in the region of interest. The resulting change is seen to be small indicating an insensitivity of the experiment to G_n^M. (b) Same as (a) but at 134.5°. The resulting change is seen to be larger, but still small.

in this kinematic region. Similar analysis showed the effect of variation of the neutron's electric form-factor, G_n^E, to be completely negligible and indicated no significant sensitivity to the fraction of D state assumed for the initial deuteron wave function over the range of 5.2%–6.6%.

More complete and sophisticated calculations than those done using McGee's work were done by Arenhövel and Leidemann for direct comparison to the cross sections measured in the present experiment. Since the theory behind these calculations has been described in detail previously[24,25] we will give just a short review of the essential ingredients. Only the two-body breakup process is considered, thus limiting the theory to the energy region below pion production threshold. The initial deuteron and the final scattering states with total angular momentum up to $j=5$ are calculated by numerical solution of the nonrelativistic Schrödinger equation using the Paris potential. For higher partial waves the final state interaction is neglected. Isobar configurations [$N-\Delta$, $\Delta-\Delta$, and $N-N(1470)$] are calculated in the impulse approximation which is considered quite reliable in this energy region.

The electromagnetic currents considered include a normal current (N), a regularized π-meson exchange current, and an isobar components contribution (IC) as described in Ref. 24. In addition to the true one-body current, the normal current also includes that part of the meson exchange current included by the Siegert theorem due to the presence of charge exchange terms in the potential. In this respect Arenhövel's normal current contributions resemble the calculation based upon the work of McGee. However, they differ in that, unlike the McGee calculations, Arenhövel's N term includes the effect of final state interactions and part of the exchange currents. The two calculations also differ in that McGee's formalism is covariant while Arenhövel's calculation is nonrelativistic except for kinematics. This

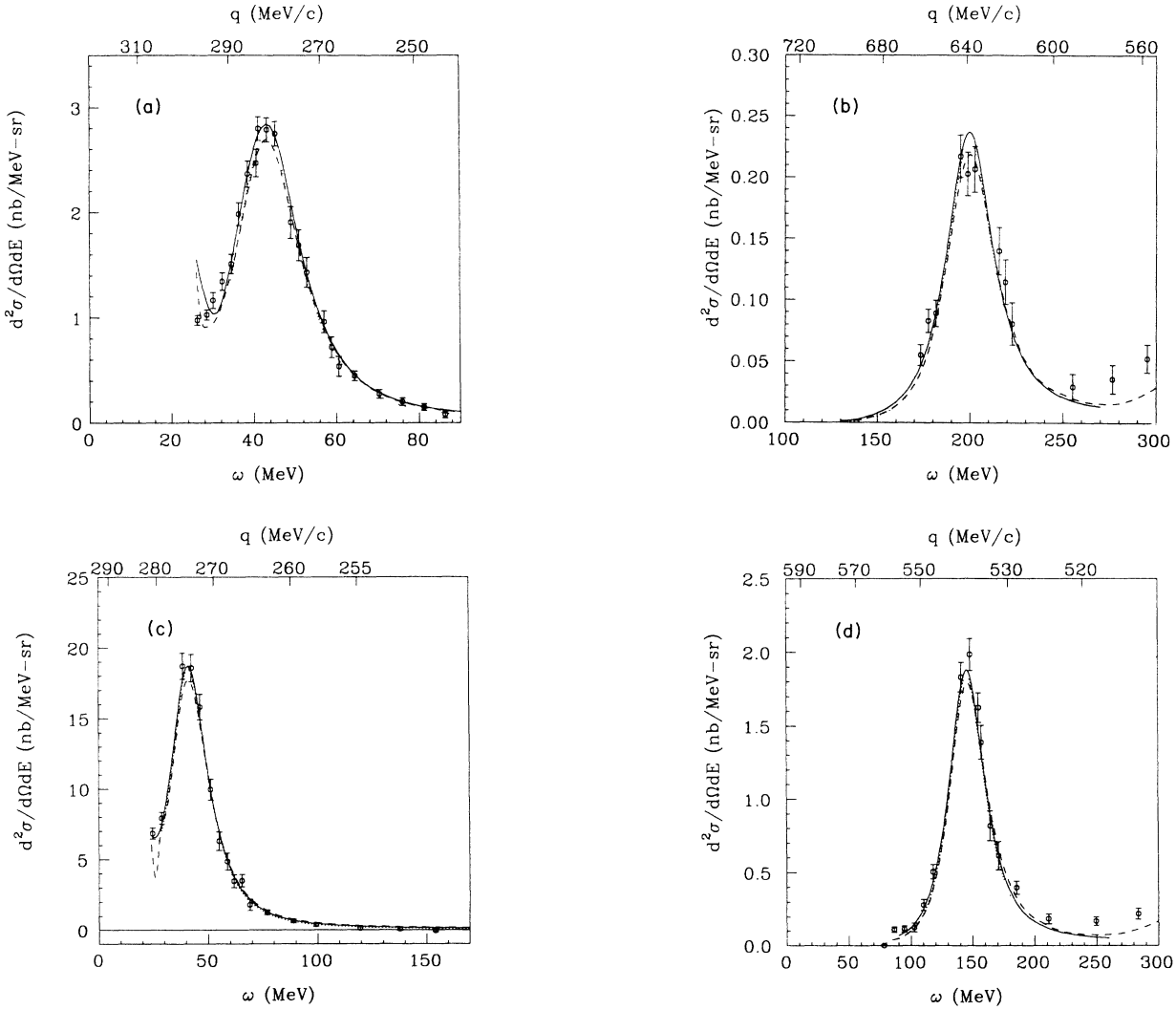

FIG. 8. These figures illustrate the effects of FSI and MEC upon the normal current calculations of Arenhövel. They also permit comparison of the full calculations of Arenhövel and Laget with the present data at the kinematic extremes of the measurements. The points represent the radiatively unfolded results of the present measurement, the solid line is the prediction of Arenhövel (Refs. 24 and 25) and the dashed curve is the prediction of Laget (Ref. 16). The dotted curve shows Arenhövel's normal current contribution (N). (a) 174 MeV 134.5°, (b) 444 MeV 134.5°, (c) 293 MeV 60°, (d) 596 MeV 60°.

difference is not expected to be significant for $q^2 < 25$ fm^{-2}. Figure 8 shows comparisons of Arenhövel and Leidemann's predictions to the actual radiatively unfolded cross sections determined in the present experiment. Agreement is generally excellent over the range of applicability of the calculation, i.e., up to the pion production threshold.

The calculations of Laget,[16] which were also performed at the kinematics of the measurements of the present work, differ fundamentally from those of Arenhövel. While Arenhövel calculates the matrix elements of the electromagnetic operator between the deuteron bound state and the final-state wave function, and expands the amplitude in terms of multipoles, Laget uses a diagrammatic approach, expanding the amplitude as a set of a few relevant diagrams where the virtual photon interacts with the basic ingredients (nucleons, pions, and Δ's) of the nuclear dynamics. The final state interactions are taken into account explicitly in diagrams where the nucleons rescatter in *S*, *P*, and *D* waves. It should be noted that *D* waves were considered here in addition to the *S* and *P* waves considered in Ref. 16. Also, the numerical values of the half-off-shell matrix elements are used,[17] rather than the phenomenological parametrization used in Ref. 16. Thus Laget's impulse approximation (IA) results cannot be directly compared to Arenhövel's normal current part of the interaction as the latter includes final state interactions and exchange currents while the former does not.

The Siegert terms are not included in Laget's calculations; rather gauge invariance is enforced by the explicit inclusion of all meson exchange diagrams in the MEC

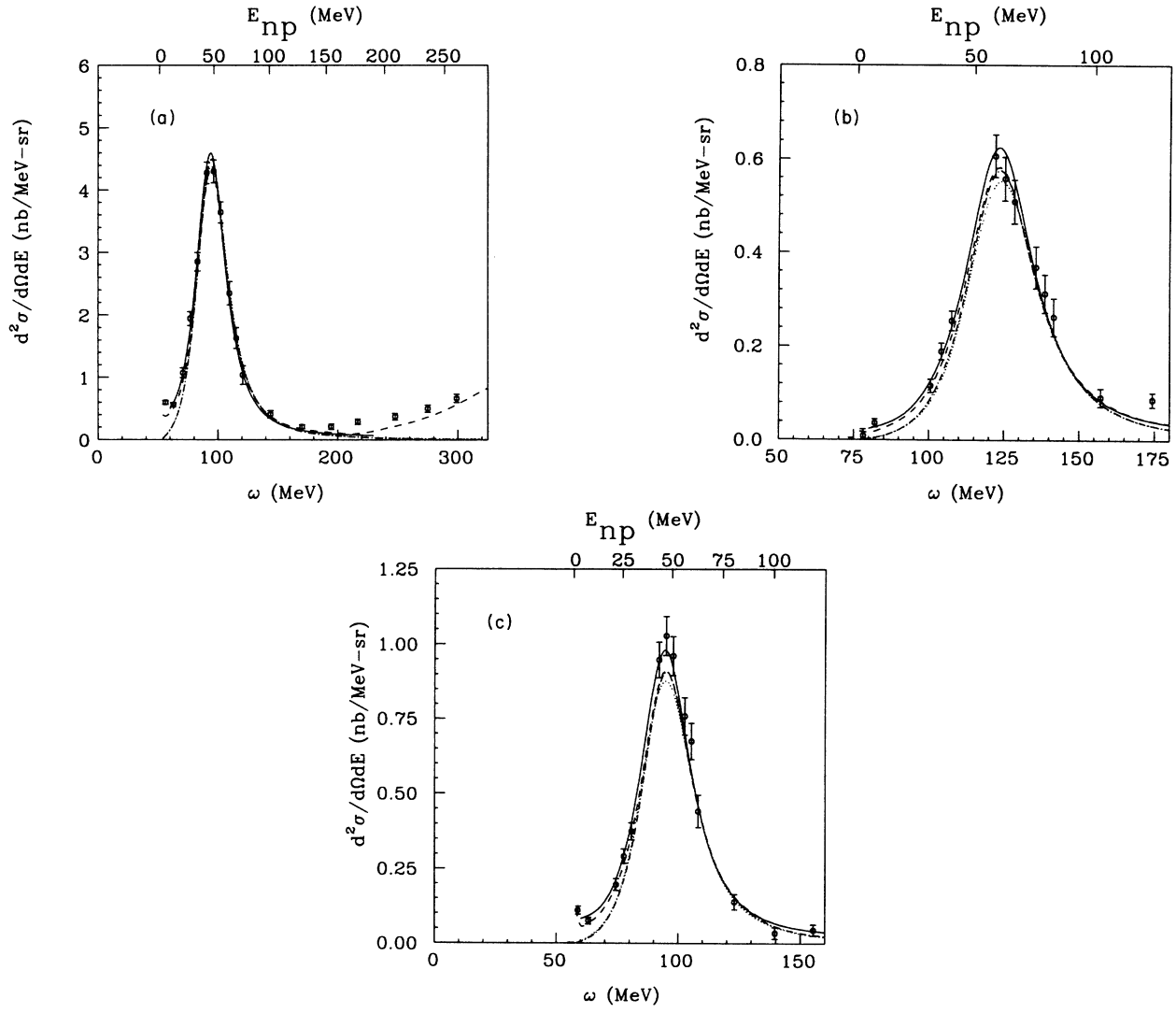

FIG. 9. These figures illustrate the effects of FSI and MEC upon the impulse current calculations of Laget. They also permit comparison of the full calculations of Arenhövel and Laget with the present data at several kinematic points of the measurements. Additionally, the calculation of McGee is shown to illustrate its similarity to Laget's impulse approximation. The points represent the radiatively unfolded results of the present measurement, the solid line is the prediction of Arenhövel (Refs. 24 and 25) and the dashed curve is the prediction of Laget (Ref. 16). The dash-dot curves show Laget's impulse approximation and the dotted curves show the calculation based on McGee's work (Ref. 11). The top scale gives the kinetic energy of the recoiling nucleons their center of mass frame. (a) 465 MeV 60°, (b) 328 MeV 134.5°, (c) 278 MeV 134.5°.

corrections. Thus no meson exchange current effects are included in Laget's IA results. Laget's IA results are directly comparable to the McGee calculations. The two are found to generally agree within a few percent, with the largest differences appearing at low energy and back angle, as seen in Fig. 9. Figures 8–10 show Laget's complete results compared to the present measurements. The data are found to be systematically higher than these predictions in the quasielastic region although qualitative agreement of the shape is good. Although individual differences between the data points and the Laget calculation are generally small compared to the statistical error, the consistent difference in one direction indicates that the differences are not merely statistical fluctuations. The pion production contribution is computed according to Ref. 18.

In view of this systematic disagreement in magnitude between the calculation of Laget and the present measurement, it may be appropriate to elaborate upon the estimated systematic error assigned to the overall normalization of the measurement. This is further motivated by a recent measurement[26] of 180° electron scattering which suggests that the calculation of Arenhövel overestimates the transverse response function by as much as 12% in the region in which the present measurement agrees with the calculation.

As mentioned earlier, the normalization constant was determined by comparing the ^{3}He elastic cross sections determined in this experiment to those obtained in a previous experiment.[20] The normalization constant thus determined, 1.06, also was reasonably consistent, within a few percent, with the comparisons of the ^{1}H and ^{4}He with a variety of previously published results, so an overall normalization constant of 1.06 ± 0.03 was adopted for all targets, including ^{2}H. No apparent mechanism would give a different normalization at back angles, nor was any indication of this seen in the elastic cross section comparison.

Since the different targets were measured sequentially at each spectrometer setting, and since the length of each target seen by the spectrometer was determined by the slits, rather than by the target vessel, the only obvious possible source of a target-to-target variation in the normalization is the gas pressure. The targets were pressurized to approximately 1500 psi then permanently sealed at the CMB-6 division of Los Alamos National Laboratory (LANL) where they were constructed. The pressures at the time of sealing were individually measured and recorded and are believed to be accurate to a fraction of 1%.

The ^{2}H elastic measurements were not originally used in the determination of the normalization constant because the proximity of the breakup threshold made it difficult to determine the elastic cross section. The relatively poor resolution resulting from the use of the nondispersed beam made it necessary to integrate the elastic peaks over a significant energy range before applying the radiative correction, and this was not possible for ^{2}H. In spite of this, in order to provide an independent check of the ^{2}H normalization, a study was made of the effect of integration over a small energy bin. It was found, for ^{3}He and ^{4}He, that the error introduced in the determination of cross section by integration over only 1.5 MeV below the elastic peak was an underestimation of the radiatively corrected cross section by about 3% when compared to determinations made with a series of lower cutoff energies. To correct for this, the ^{2}H spectra were integrated to 1.5 MeV, the integral was radiatively corrected in the normal manner then multiplied by the correction factor of 1.03. These results were then compared to previous measurements of ^{2}H elastic scattering.[22] This independent determination yielded a normalization constant of 1.02. Again, no evidence was seen that the factor depended upon scattering angle. This value should be considered to be a lower limit for the normalization constant, as any background contamination from deuteron breakup would cause this determination to yield an underestimate. As no contradiction was found, the better estimate of 1.06 ± 0.03 was taken to be the proper normalization constant for ^{2}H.

Since the normalization of the present experiment does not appear to be uncertain, the disagreement between the present results and those of Ref. 26 appears to be real. Comparison of our results[27] for ^{3}He and ^{4}He to previous measurements[28,29] at the few points of kinematic overlap does not suggest a problem in the normalization of the present work. On the other hand, comparison[30] of the deuterium elastic cross sections extracted from the data of Ref. 26 with that of recent high accuracy data[31] suggest a systematically low normalization of the data of Ref. 26, at least at high momentum transfer. We conclude that the discrepancy between the present data and that of Ref. 26 results from an unknown systematic error in the latter work, and that the systematic error on the present data is only 3%, as quoted above.

RESULTS

Figure 8 compares the data from the present experiment to Arenhövel and Leidemann's calculation over some of the kinematic region covered in the experiment. In each figure the normal current contribution is shown as well as the total calculation. The difference between these curves represents the calculated contribution from MEC and IC. These corrections are seen to be relatively small compared to the statistical error on the radiatively corrected data, reflecting the fact that the deuteron is very loosely bound so the interaction is reasonably well described by normal currents. The exceptions to this are the low energy-loss regions at low incident energy. At 293 MeV and 60° the data are seen to suggest agreement with the full calculation although the statistical errors are still comparable to the total correction.

Figure 9 compares the contributions of the components of the Laget calculation to the present data for a selection of kinematic points. The differences between the Born curves and the DWIA curves give a measure of the effects of final state interactions. FSI effects are seen to be largest in the breakup-threshold region where the total kinetic energy in the final n-p system is small. They are also significant at all energy loss for low q. Figure 10 illustrates the longitudinal and transverse contributions to the cross section, as calculated by Laget, over typical

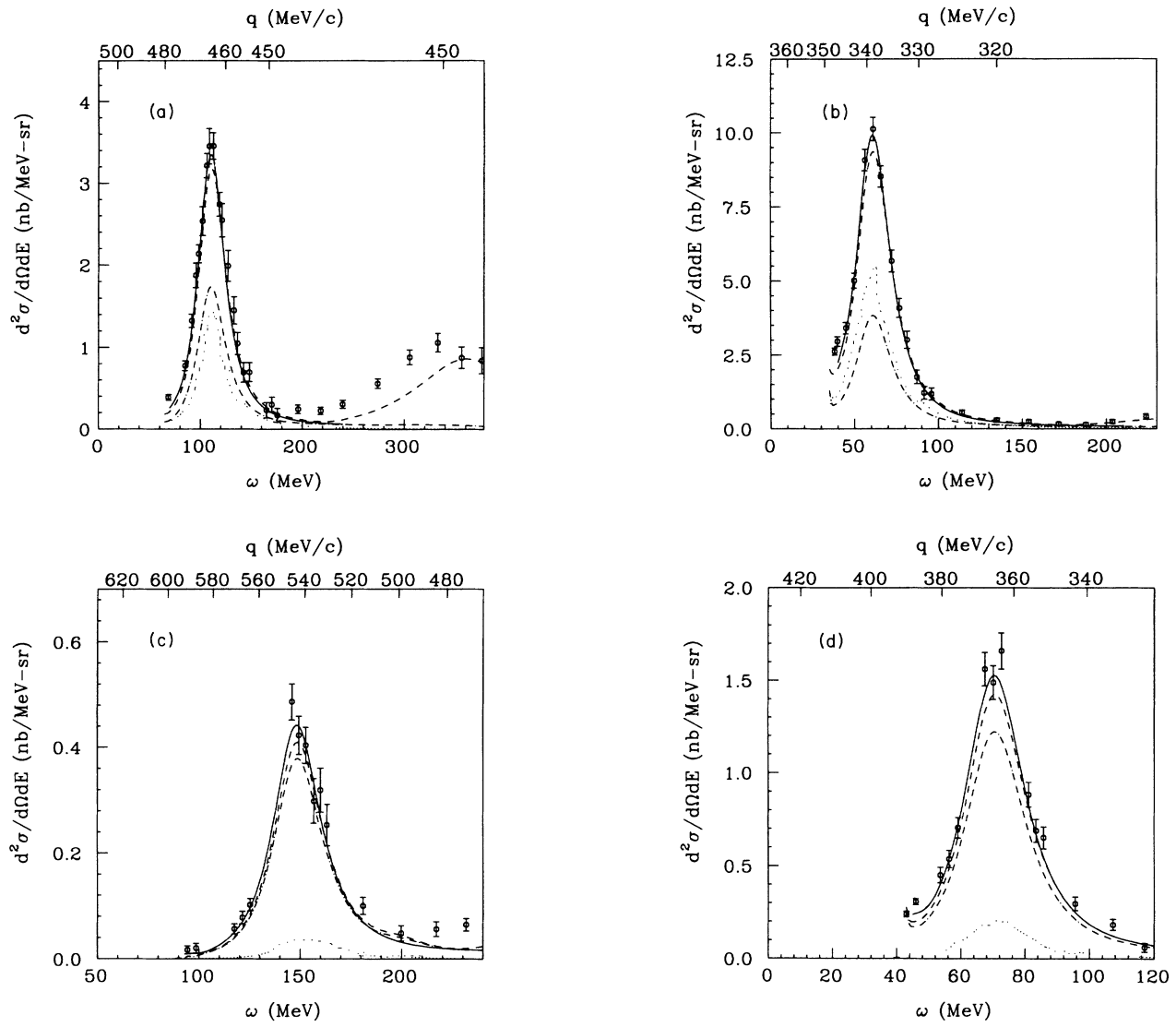

FIG. 10. These figures illustrate the relative contributions of the longitudinal and transverse response functions. Transverse contributions dominated at the back angle while the two contributions tend to be more equal at the forward angle. The figures also permit comparison of the full calculations of Arenhövel and Laget with the present data at several kinematic points of the measurements. In these figures the points represent the radiatively unfolded results of the present measurement, the solid line is the prediction of Arenhövel (Refs. 24 and 25) and the dashed curve is the prediction of Laget (Ref. 16). The dotted curve shows Laget's estimate of the longitudinal contribution, and the dot-dash curve shows his estimate of the transverse contribution. (a) 510 MeV 60°, (b) 366 MeV 60°, (c) 368 MeV 134.5°, (d) 233 MeV 134.5°.

kinematic regions covered in the experiment. The contributions of the transverse response function dominate at the back angle, especially at higher energies. In principle, this simplifies the extraction of the transverse response function since the back-angle data require only small corrections to subtract off the longitudinal part. Unfortunately, due to count rate considerations, the statistical errors at the back angle are fairly large. At forward angles the longitudinal contribution is more significant, although the transverse is somewhat larger at high energy. The error on the extraction of longitudinal response functions is therefore quite large at high energies since statistical errors on the back-angle data are magnified in the Rosenbluth extraction of this contribution.

Figure 11 compares the extracted longitudinal and transverse response functions along the kinematic lines of the 134.5° data to the predictions of Arenhövel and Laget. The data is seen to be in good agreement with both predictions. Unfortunately, the predictions are sufficiently similar and the error bars on the data are sufficiently magnified by the radiative correction and separation process that it is impossible to select one calculation over the other. It is especially interesting to note that neither the longitudinal nor transverse response functions in the dip regions shows any evidence of

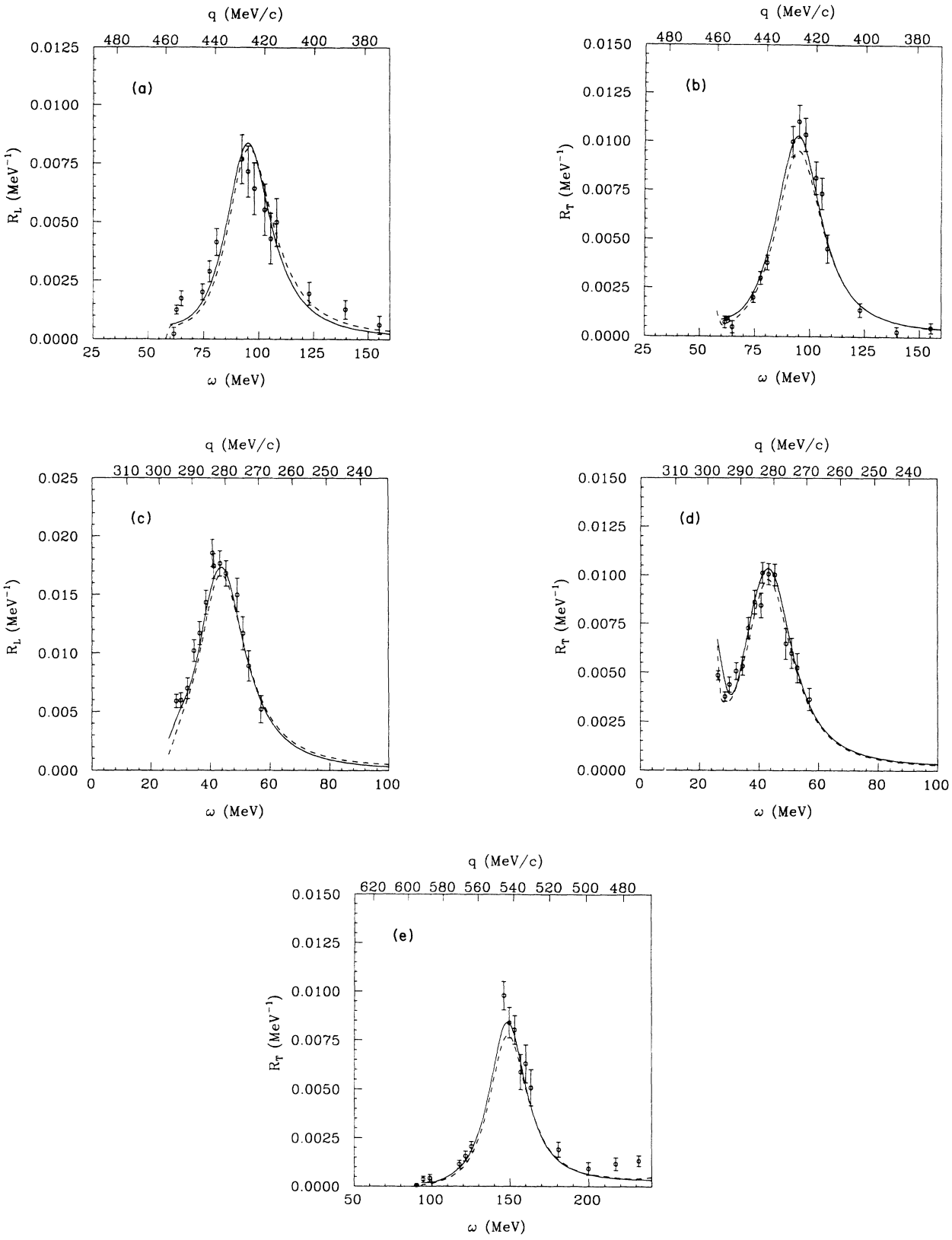

FIG. 11. In these figures the points represent the separated (longitudinal or transverse) response function found from the present measurement, the solid lines are the predictions of Arenhövel (Refs. 24 and 25) and the dashed lines are the predictions of Laget (Ref. 16). Each spectrum represents a slice through the response surface along one of the kinematic curves of a measurement at 134.5° (the solid curves of Fig. 1). (a) R_L, (b) R_T (for 279 MeV, 134.5° kinematics); (c) R_L, (d) R_T (for 174 MeV, 134.5° kinematics); (e) R_T (for 368 MeV, 134.5° kinematics).

significant enhancement over prediction, in contrast to the present situation in heavier nuclei.[1-3] Both the longitudinal and the transverse response functions at 233 and 279 MeV have sufficiently good statistics to absolutely preclude the existence of an excess cross section on the order of 20% of the height of the quasielastic peak, like that seen[3] in ^{12}C. This is seen even more clearly in the cross sections themselves, Figs. 8–10.

It should be noted that actually performing a Rosenbluth separation provides no fundamentally new information about the relationship between the data and theory which cannot be seen by comparing the cross section measurements. In fact, in a case like the present one in which statistical errors are dominant, the propagation of errors inherent in the separation may tend to cloud the comparison. The only requirement for a reasonable evaluation of both the longitudinal and transverse components of a calculation is a body of data which covers the same q-ω region at two or more significantly different angles. A theory which correctly predicts all these cross sections will correctly predict the extracted response functions. There are, however, some advantages in actually extracting the response functions. There may be important diagnostic information revealing systematic errors if the extracted values are found to be negative or if multiangle separations are found not to yield straight lines. Additionally, the error bars on the extracted response functions give the measure of how closely the separate longitudinal and transverse predictions of the calculation are actually being tested by the data.

The dip region is extremely sensitive to uncontrolled systematic errors and background. These would generally have the effect of increasing cross sections and therefore increasing at least one response function. The fact that such small results were obtained shows the data to be relatively free of errors and backgrounds, at least in the low momentum transfer region. One exception to the rule that backgrounds generally artificially increase measured cross sections would be a contamination in the positive-polarity spectrum. If such a background were then misidentified as pair-produced positrons, and subtracted from the negative spectrum, the resulting cross section would then be too low. In the present experiment no such positron subtraction was performed, but this is common practice in analysis of inelastic scattering experiments and should be carefully evaluated.

CONCLUSIONS

Cross sections have been measured for inelastic electron scattering from the deuteron over a wide range of kinematics. A sufficient body of data have been taken to permit the first model-free radiative correction of such measurements on the deuteron. Good agreement has been found with the calculations of Arenhövel at both forward and back angles. The calculations of Laget are systematically somewhat lower than the measured values.

Data have been taken at two angles over a large kinematic region, allowing Rosenbluth separation to be performed. Longitudinal and transverse response functions have been extracted from the data and are found to agree with the Arenhövel calculation (as follows from the agreement at both forward and back angles). This represents the first model-free separation of these response functions in the deuteron. The agreement of the transverse response function with the predictions of Arenhövel is in direct disagreement with previously published 180° scattering measurements.[26] For the reasons given above, we believe the normalization of the present measurement to be correct, indicating a problem in the normalization of data in Ref. 26.

The success of this separation confirms that such separations can be performed in this kinematic region. The statistical errors on the separated response functions are large, especially at high momentum transfer. Further work in this area to reduce the statistical errors and extend measurements to higher q is in progress. Great care will also be required to keep the systematic errors small. A good understanding of scattering from the deuteron and other light nuclei is essential, however, if results in larger nuclei are to be understood.

ACKNOWLEDGMENTS

The authors are grateful to the staff of the Bates Linear Accelerator Lab for their cooperation throughout the experiment, and particularly to Phil Sargent and Jay Flanz for their efforts on upgrading and operating the machine. This work was funded by the U.S. Department of Energy under Contracts DE-AC02-76ER03069 and DE-FG0586ER40261, and by the National Science Foundation under Grant PHY-8518521.

---

*Present address: Carnegie-Mellon University, Pittsburgh, PA 15213.
†Present address: Lund Institute of Technology, Lund, Sweden.
‡Present address: University of Pittsburgh, Pittsburgh, PA 15260.
§Present address: University of Virginia Medical School, Charlottesville, VA 22901.
**Present address: Westinghouse, Columbia, MD 21145.
††Present address: CEBAF, Newport News, VA 23606.

[1]E. J. Moniz *et al.*, Phys. Rev. Lett. **26**, 445 (1971).
[2]R. M. Altemus *et al.*, Phys. Rev. Lett. **44**, 965 (1980); M. Deady *et al.*, Phys. Rev. C **28**, 631 (1983).
[3]P. Barreau *et al.*, Nucl. Phys. **A402**, 515 (1983).
[4]B. P. Quinn, Ph. D. thesis Massachusetts Institute of Technology, 1984 (unpublished).
[5]K. A. Dow, Bull. Am. Phys. Soc. **34**, 1052 (1987); K. F. Von Reden, *ibid.* **34**, 1059 (1987).
[6]E. L. Lomon and H. Feshback, Ann. Phys. **48**, 94 (1968).
[7]M. Lacombe *et al.*, Phys. Rev. C **21**, 861 (1980).
[8]M. R. Yearian and R. Hofstadter, Phys. Rev. **110**, 152 (1958); C. W. Akerlof, K. Berkelman, G. Rouse, and M. Tigner, *ibid.* **135B**, 810 (1964); E. B. Hughes, T. A. Griffy, M. R. Yearian,

and R. Hofstader, *ibid.* **139B**, 458 (1965); P. Stein *et al.*, Phys. Rev. Lett. **16**, 592 (1966); W. Albrecht *et al.*, Phys. Lett. **26B**, 642 (1968); K. M. Hanson *et al.*, Phys. Rev. D **8**, 753 (1973).
[9]L. Durand, Phys. Rev. **115**, 1020 (1959).
[10]J. Nuttall and M. Whippman, Phys. Rev. **130**, 2495 (1963); M. Gourdin, M. LeBellac, F. M. Renard, and J. Trân Thanh Vân, Phys. Lett. **18**, 73 (1965); P. Breitenlohner, K. Hölzl and P. Kocevar, *ibid.* **19**, 54 (1965); F. M. Renard, J. Trân Thanh Vân and M. Le Bellac, Nuovo Cimento **38**, 552 (1965); **38**, 565 (1965); **38**, 1688 (1965).
[11]I. J. McGee, Phys. Rev. **158**, 1500 (1967).
[12]I. J. McGee, Phys. Rev. **161**, 1640 (1967).
[13]W. Fabian and H. Arenhövel, Nucl. Phys. **A258**, 461 (1976).
[14]G. G. Simon *et al.*, Phys. Rev. Lett. **37**, 739 (1976).
[15]G. G. Simon *et al.*, Nucl. Phys. **A324**, 277 (1979).
[16]J. M. Laget, Can. J. Phys. **62**, 1046 (1984).
[17]J. M. Laget, Phys. Rev. C **35**, 832 (1987).
[18]J. M. Laget, Phys. Lett. **151B**, 325 (1985).
[19]T. deForest, Jr. and J. D. Walecka, Adv. Phys. **15**, 1 (1966).
[20]P. Dunn, Ph. D. thesis, Harvard University, 1980 (unpublished).
[21]L. W. Mo and Y. S. Tsai, Rev. Mod. Phys. **41**, 205 (1969).
[22]S. Stein *et al.*, Phys. Rev. D **12**, 1884 (1975).
[23]G. Hohler *et al.*, Nucl. Phys. **B114**, 505 (1976) (Fit 8.2 was employed for nucleon form factors.)
[24]W. Fabian and H. Arenhövel, Nucl. Phys. **A314**, 253 (1979).
[25]H. Arenhövel, Nucl. Phys. **A384**, 287 (1982).
[26]B. Parker *et al.*, Phys. Rev. C **34**, 2354 (1986).
[27]S. A. Dytman *et al.* submitted to Phys. Rev. C.
[28]J. S. McCarthy, I. Sick, R. R. Whitney, and M. R. Yearian, Phys. Rev. C **13**, 712 (1976).
[29]C. Marchand *et al.*, Phys. Lett. **B153**, 29 (1985).
[30]B. Parker, Ph. D. thesis, University of Massachusetts, 1985, (unpublished).
[31]S. Auffret *et al.*, Phys. Rev. Lett. **54**, 649 (1985).